Timing, carrier frequency and phase recovery for OFDM and Nyquist signals using a mean modulus algorithm

R. Schmogrow,[1,3,4,*] B. Nebendahl,[2] A. Josten,[3] P.C. Schindler,[1] C. Koos,[1] W. Freude,[1] and J. Leuthold[1,3]

[1]*Institute of Photonics and Quantum Electronics (IPQ), Karlsruhe Institute of Technology (KIT), Germany*
[2]*Agilent Technologies, Boeblingen, Germany*
[3]*ETH Zurich, Institute of Electromagnetic Fields (IEF), Zurich, Switzerland*
[4]*Now with: Infinera Corporation, Sunnyvale, California, USA*
[*]*RSchmogrow@infinera.com*

Abstract: Efficient algorithms for timing, carrier frequency and phase recovery of Nyquist and OFDM signals are introduced and experimentally verified. The algorithms exploit the statistical properties of the received signals to efficiently derive the optimum sampling time, the carrier frequency offset, and the carrier phase. Among the proposed methods, the mean modulus algorithm (MMA) shows a very robust performance at reduced computational complexity. This is especially important for optical communications where data rates can exceed 100 Gbit/s per wavelength. All proposed algorithms are verified by simulations and by experiments using optical *M*-ary QAM Nyquist and OFDM signals with data rates up to 84 Gbit/s.

OCIS codes: (060.0060) Fiber optics and optical communications; (060.1660) Coherent communications; (060.2330) Fiber optics communications.

References and links

1. G. Bosco, V. Curri, A. Carena, P. Poggiolini, and F. Forghieri, "On the performance of Nyquist-WDM terabit superchannels based on PM-BPSK, PM-QPSK, PM-8QAM or PM-16QAM subcarriers," J. Lightwave Technol. **29**(1), 53–61 (2011).
2. R. Schmogrow, M. Winter, M. Meyer, D. Hillerkuss, S. Wolf, B. Baeuerle, A. Ludwig, B. Nebendahl, S. Ben-Ezra, J. Meyer, M. Dreschmann, M. Huebner, J. Becker, C. Koos, W. Freude, and J. Leuthold, "Real-time Nyquist pulse generation beyond 100 Gbit/s and its relation to OFDM," Opt. Express **20**(1), 317–337 (2012).
3. W. Shieh, H. Bao, and Y. Tang, "Coherent optical OFDM: theory and design," Opt. Express **16**(2), 841–859 (2008).
4. J. Leuthold and W. Freude, "Optical OFDM and Nyquist multiplexing," in *Optical Fiber Telecommunications Volume VIB: Systems and Networks* (Optics and Photonics), I. Kaminow, T. Li, A.E. Willner, eds. (Academic Press, 2013).
5. S. D. Personick, "Receiver design for digital fiber optic communication systems, I," Bell Syst. Tech. J. **52**(6), 843–874 (1973).
6. F. M. Gardner, "A BPSK/QPSK timing-error detector for sampled receivers," IEEE Trans. Commun. **34**(5), 423–429 (1986).
7. H. Meyr, M. Moeneclaey, and S. A. Fechtel, *Digital Communication Receivers: Synchronization, Channel Estimation, and Signal Processing* (Wiley, 1997).
8. N. D'Andrea and U. Mengali, "A simulation study of clock recovery in QPSK and 9QPRS systems," IEEE Trans. Commun. **33**(10), 1139–1142 (1985).
9. M. Oerder and H. Meyr, "Digital filter and square timing recovery," IEEE Trans. Commun. **36**(5), 605–612 (1988).
10. M. Yan, Z. Tao, L. Dou, L. Li, Y. Zhao, T. Hoshida, and J. Rasmussen, "Digital clock recovery algorithm for Nyquist signal," in Optical Fiber Communication Conference, OSA Technical Digest (online) (Optical Society of America, 2013), paper OTu2I.7.
11. A. Viterbi and A. Viterbi, "Nonlinear estimation of PSK-modulated carrier phase with application to burst digital transmission," IEEE Trans. Inf. Theory **29**(4), 543–551 (1983).
12. T. M. Schmidl and D. C. Cox, "Robust frequency and timing synchronization for OFDM," IEEE Trans. Commun. **45**(12), 1613–1621 (1997).

#205525 - $15.00 USD Received 3 Feb 2014; revised 27 Mar 2014; accepted 27 Mar 2014; published 10 Apr 2014

13. R. Bouziane, R. Schmogrow, D. Hillerkuss, P. A. Milder, C. Koos, W. Freude, J. Leuthold, P. Bayvel, and R. I. Killey, "Generation and transmission of 85.4 Gb/s real-time 16QAM coherent optical OFDM signals over 400 km SSMF with preamble-less reception," Opt. Express **20**(19), 21612–21617 (2012).
14. J. E. Volder, "The CORDIC Trigonometric Computing Technique," IRE Trans. Electron. Comput. **EC-8**(3), 330–334 (1959).
15. C. R. Johnson, Jr., P. Schniter, T. J. Endres, J. D. Behm, D. R. Brown, and R. A. Casas, "Blind equalization using the constant modulus criterion: A review," Proc. IEEE **86**(10), 1927–1950 (1998).
16. R. Schmogrow, D. Hillerkuss, M. Dreschmann, M. Huebner, M. Winter, J. Meyer, B. Nebendahl, C. Koos, J. Becker, W. Freude, and J. Leuthold, "Real-time software-defined multiformat transmitter generating 64QAM at 28 GBd," IEEE Photon. Technol. Lett. **22**(21), 1601–1603 (2010).

1. Introduction

Clock and carrier recovery are crucial tasks when coherently receiving data transmitted over optical links. Although a variety of synchronization algorithms are known from wireless and wireline communications, it is the use of extremely high data rates (frequently beyond 100 Gbit/s) in optical links which represents a big challenge. With the advent of computationally expensive pulse-shaping techniques like Nyquist signaling [1] [2] and orthogonal frequency division multiplexing (OFDM) [3] for optical networks, standard blind synchronization methods fail. However, Nyquist and OFDM signaling have become important as they allow for coding at highest spectral efficiency [4]. Nyquist signals comprise sinc-like pulses which overlap in time but do not show any inter-symbol interference (ISI). Such sinc-like pulses are infinitely extended in time but have a finite "raised-cosine" spectrum [5], the shape and width of which are described by the roll-off factor β. On the other hand, OFDM signals have finitely extended rect-shaped symbols with infinitely extended sinc-shaped subcarrier (SC) spectra that overlap in frequency. The SC spectra are separated by the reciprocal symbol duration, are orthogonal and hence free of inter-channel interference (ICI).

Timing recovery (also: clock recovery) and carrier recovery methods can be grouped into feedforward and feedback techniques. In both cases, the actual value of frequency, phase or sampling time has to be estimated. This information is represented by a control variable, which either leads to a feedforward correction, or gives the actual value in a feedback loop.

In the past, for single carrier formats such as Nyquist signals, a number of methods have been proposed to provide data for synchronizing the receiver (Rx) clock to the Tx clock. One way to find the proper timing information is to use square-law detectors [6] [7], i.e., the modulus of the received time domain signal is squared. However, this algorithm is not applicable for Nyquist pulses with a small roll-off factor $\beta \approx 0$ [6] [7]. A solution suitable for signals with small β is to use absolute-value rectifiers [8]. The distorted signal can then be fed to a fast Fourier transform (FFT) in order to obtain the clock frequency and phase information from the spectrum with peaks at the clock frequency [9] [10].

In a next step, carrier recovery is performed, usually using the well-known Viterbi-Viterbi algorithm [11] that requires a proper timing synchronization in advance. The Viterbi-Viterbi method provides both the carrier frequency and the carrier phase offset.

For multicarrier signals such as with OFDM, the Schmidl-Cox algorithm [12] is widely used. It computes the correlation of training patterns to provide timing and carrier frequency information at the same time.

In this paper we propose and experimentally demonstrate simple and highly efficient blind algorithms for timing information recovery as well as for carrier frequency and phase estimation. In particular, it is shown that our mean modulus algorithm (MMA) is well suited for both Nyquist and OFDM signals. It can be used to extract clock, carrier frequency and phase while featuring a low computational complexity [2] [13].

The paper is organized as follows: We first present an intuitive view on the operation principle followed by the theoretical description of the basic recovery techniques in a generalized form (applicable to both Nyquist and OFDM signals). Next, we compare the MMA to the well-known CMA. Finally, we discuss the experimental setup and apply the algorithms to OFDM signals with 128 SCs and Nyquist pulses with various roll-off factors β and data rates of up to 84 Gbit/s.

#205525 - $15.00 USD Received 3 Feb 2014; revised 27 Mar 2014; accepted 27 Mar 2014; published 10 Apr 2014

2. Operation principle

In this section we give an intuitive explanation on the operation principles of the clock recovery, which is investigated in more detail further below. Exemplarily, we show the operation principle by studying the color-coded eye-diagrams and mean values (black dashed lines) of two signals with different pulse shapes as a function of time and symbol period T_s, see Fig. 1.

The amplitude envelope of the first signal is plotted in Fig. 1(a), upper row. It was obtained from a binary phase shift keyed (BPSK) signal with a sinc-like pulse shape (also known as a "raised-cosine" pulse due to its raised-cosine spectrum). The amplitude envelope of the second signal is plotted in Fig. 1(b), upper row. This time we evaluate a BPSK signal with a Nyquist sinc pulse shape. The mean value of the amplitude envelopes is a straight line, and no timing information can be derived. In a next step, we square the amplitudes [6] [7], so that power envelopes are obtained, see Fig. 1, lower row. To find the ideal sampling position with the maximum eye opening we now take the mean of the power envelope. It can be seen that in the case of a "raised-cosine" pulse shape, the mean power (black dashed line) is at its maximum at the ideal sampling position. Unfortunately, this simple operation does not help to find the ideal sampling time for the sinc-shaped signal, because here the mean power is constant for all possible sampling instances. This will be theoretically discussed in Section III where we show scenarios in which the mean power algorithm (MPA) performs well, and where we investigate its limitations.

In Section 4 we will then show how introducing a nonlinear operation [7] [8] prior to the averaging process will allow finding the ideal sampling time and carrier frequency even for sinc-shaped signals. It will be demonstrated that a variety of signals can be handled, while keeping the computational effort reasonably low.

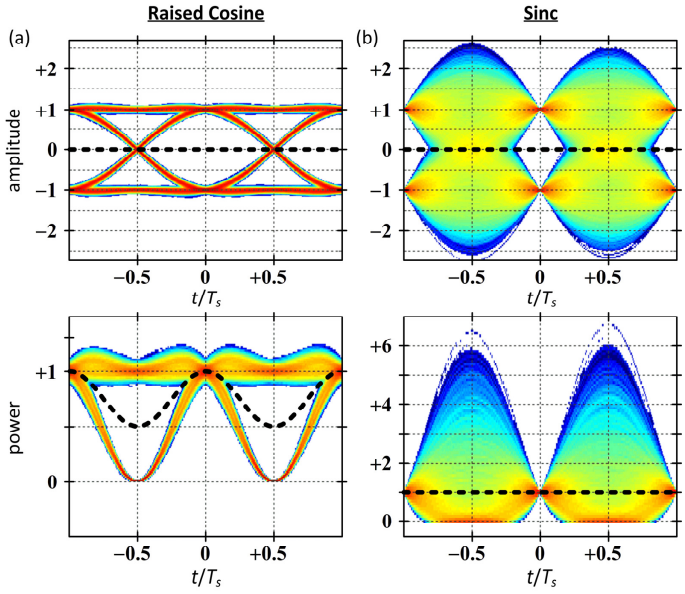

Fig. 1. Color-coded eye-diagrams and mean values (black dashed lines) as a function of time (T_s: symbol period). The plots are obtained from amplitudes (upper row) and powers (lower row) of binary phase shift keyed (BPSK) signals with (a) a sinc-like pulse shape with raised-cosine spectrum and (b) a sinc-pulse shape. While the mean power of signals with "raised-cosine" pulses (a) does reveal timing information, the signals comprising sinc-shaped pulses (b) produce large overshoots leading to a constant mean power for all t.

#205525 - $15.00 USD Received 3 Feb 2014; revised 27 Mar 2014; accepted 27 Mar 2014; published 10 Apr 2014

3. The mean power algorithm for timing and frequency recovery

For deriving efficient methods for successfully recovering timing and carrier information from arbitrary Nyquist and OFDM signals, we now take a theoretical approach. In this section, we investigate to what extend the mean power of a signal can be used to obtain information with respect to carrier frequency offset and timing. First, sinc-shaped pulses/spectra (Nyquist/OFDM) are investigated, and then rect-shaped spectra/pulses (Nyquist/OFDM) will be discussed.

3.1 Nyquist timing and OFDM frequency recovery

Generally, a sinc-like "raised-cosine" Nyquist multicarrier signal $s_{\mathrm{Nyquist}}(t)$ in the time domain, or an OFDM signal $s_{\mathrm{OFDM}}(f)$ in the frequency domain is defined by [2]

$$\begin{aligned} s_{\mathrm{Nyquist}}(t) &= \sum_{i=0}^{N-1}\sum_{k=-\infty}^{+\infty} c_{ik}\exp\left(+\mathrm{j}2\pi\frac{it}{T_s}\right)\mathrm{sin\,cl}\left(\frac{t}{T_s}-k\right), \\ s_{\mathrm{OFDM}}(f) &= \frac{1}{F_s}\sum_{i=-\infty}^{+\infty}\sum_{k=0}^{N-1} c_{ik}\exp\left(-\mathrm{j}2\pi\frac{if}{F_s}\right)\mathrm{sin\,c}\left(\frac{f}{F_s}-k\right). \end{aligned} \tag{1}$$

The quantities c_{ik} are the complex modulation coefficients, T_s is the symbol period in the time domain, and F_s the symbol period in the frequency domain, i.e., the spacing of the OFDM subcarriers (SC). The sinc-like (sincl) and the sinc-functions are defined in the following:

$$\begin{aligned} \mathrm{sin\,cl}\left(\frac{z}{Z}\right) &= \mathrm{sin\,c}\left(\frac{z}{Z}\right)\frac{\cos(\pi\beta z/Z)}{1-4\beta^2 z^2/Z^2} \\ \mathrm{sin\,c}\left(\frac{z}{Z}\right) &= \begin{cases} 1 & \text{for } z=0 \\ \dfrac{\sin(\pi z/Z)}{\pi z/Z} & \text{else} \end{cases} \end{aligned} \tag{2}$$

The sincl-function has a raised-cosine Fourier transform [5] with roll-off factor β and a spectral support (bandwidth) of $(1 + \beta) / Z$. Due to realization constraints, only a finite number of Q neighbors with respect to subscripts k contribute to the functions Eq. (1) for a given t or f. We also limit the number of symbols R with index i that will be considered. The expression in Eq. (1) can then be formulated in a unified form with $z = t$, $Z = T_s$ (Nyquist) or $z = f$, $Z = F_s$ (OFDM, $\beta = 0$)

$$s(z) = \sum_{k=-Q/2}^{+Q/2} c_k(z)\,\mathrm{sin\,cl}\left(\frac{z}{Z}-k\right),\quad c_k(z) = \sum_{i=-R/2}^{+R/2} c_{ik}\,\mathrm{e}^{\mathrm{j}2\pi\frac{iz}{Z}}. \tag{3}$$

The functions $c_k(z)$ are Fourier series and are represented by a finite number of $R + 1$ terms subscripted with i due to the aforementioned realization constraints. For a single-carrier Nyquist signal or for a single-symbol OFDM spectrum ($R = 0$, not a practical case!) this series reduces to one single term. Figure 2 visualizes the signal Eq. (3) for $R = 0$, $\beta = 0$, and $Q = 2$.

#205525 - $15.00 USD Received 3 Feb 2014; revised 27 Mar 2014; accepted 27 Mar 2014; published 10 Apr 2014

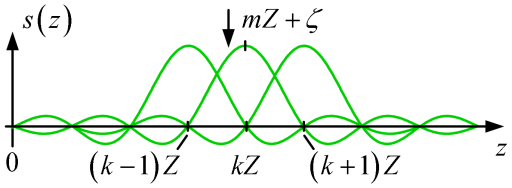

Fig. 2. Sinc-shaped pulses in time (Nyquist) or frequency domain (OFDM) as defined by the sum terms of Eq. (3) for $R = 0$ and $Q = 2$ neighbors. Pulses are separated by multiples k of the symbol period Z. The offset from the ideal sampling position mZ is named ζ.

In the following, we need to find the ideal sampling position for the reception of the signal described by Eq. (3). The ideal sampling position is located at the sincl-centers $z_m = m\,Z$, $m \in \mathbb{Z}$, see Fig. 2. Without loss of generality we set $m = 0$ and then define a so-called sampling offset ζ with respect to this ideal sampling position,

$$-0.5 < \zeta / Z \le 0.5. \tag{4}$$

From the intuitive introduction Fig. 1 we expect the optimum sampling position at $\zeta = 0$, i.e., at the position where the received signal power averaged over several samples is maximum. To show this, we now evaluate the ensemble average of the power $S(\zeta)$ of a Nyquist signal, or of an OFDM spectrum according to (Eq. (3) with $R = 0$ for a single carrier/symbol)

$$\begin{aligned} S(\zeta) = |s(\zeta)|^2 &= \sum_{k,k'=-Q/2}^{Q/2} c_k c_{k'}^* \,\mathrm{sin\,cl}\left(\frac{\zeta}{Z} - k\right)\mathrm{sin\,cl}\left(\frac{\zeta}{Z} - k'\right), \\ \overline{S(\zeta)} &= \sum_{k,k'=-Q/2}^{Q/2} \overline{c_k c_{k'}^*}\,\mathrm{sin\,cl}\left(\frac{\zeta}{Z} - k\right)\mathrm{sin\,cl}\left(\frac{\zeta}{Z} - k'\right) \\ &\approx \overline{|c_k|^2} \sum_{k=-Q/2}^{Q/2} \mathrm{sin\,cl}^2\left(\frac{\zeta}{Z} - k\right). \end{aligned} \tag{5}$$

Because $R = 0$ is assumed in Eq. (3), the received modulation coefficients c_k are independent of the offset ζ. Furthermore, the lower row of Eq. (5) only gets contributions from the dominant sincl-contributions with $k = k'$ ($\overline{c_k c_{k'}^*} = 0$ for $k \neq k'$ and $\zeta \neq 0$ with statistically independent c_k and $c_{k'}$, which results from the symmetry property of commonly used constellation diagrams), so that the double sum reduces to a single sum. The quantity $\overline{|c_k|^2}$ stands for the mean power of all complex data coefficients c_k in Eq. (3). For sinc-functions ($\beta = 0$) and large numbers of signals/symbols $Q \to \infty$, the right-hand side of Eq. (5) reduces to $\overline{|c_k|^2}$. Thus, the mean power is constant and independent from the offset ζ. For $\beta \neq 0$ and/or for sufficiently small Q, we find that computing Eq. (5) provides a maximum mean power at the optimum sampling position $\zeta = 0$. Thus, in general, the optimum sampling position can be found by averaging the power over a small number of signals/symbols leading to the mean power algorithm (MPA). For visualization purposes, we plot the mean power according to Eq. (5) for different Q and β, see Fig. 3.

#205525 - $15.00 USD Received 3 Feb 2014; revised 27 Mar 2014; accepted 27 Mar 2014; published 10 Apr 2014

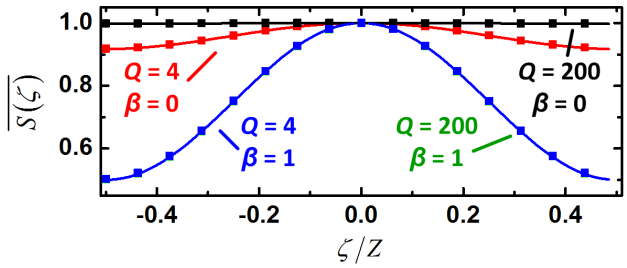

Fig. 3. For finding the ideal Nyquist sampling time or OFDM carrier frequency, the ensemble average of the power $S(\zeta)$ has been calculated (lines), simulated (solid squares), and plotted as a function of the sampling offset ζ normalized to the symbol period Z. The ideal sampling time or carrier frequency is given by $\zeta = 0$. Sinc-shaped functions with low roll-off factors β close to $\beta = 0$ only have a maximum at $\zeta = 0$ if a small number Q of neighbor symbols/spectra is included in the averaging process. For sincl-functions (having a raised-cosine spectrum) with β close to 1, the number of neighbor symbols Q is less important, because sincl-functions with larger β in Eq. (2) decay much faster than sinc-functions with $\beta = 0$.

To further support our findings, we additionally performed numerical simulations for random 64-ary quadrature amplitude modulated (64QAM) data. The analytically obtained curves (lines) and the results from simulations (squares) coincide. These general results can now be used to perform timing or carrier frequency recovery.

Timing recovery for Nyquist signals ($z = t$, $Z = T_s$, $\zeta = \tau$): The maximum of $\overline{S(\tau)}$ for a single-carrier Nyquist signal in Fig. 3 defines the correct sampling time $\tau = 0$ for the chosen pulse m. For sinc-pulses ($\beta = 0$), the number of neighbors Q must be sufficiently small for a well pronounced maximum. For sincl-pulses (having a raised-cosine spectrum with $\beta \neq 0$) even larger numbers of Q can be used.

Carrier frequency recovery for OFDM signals ($z = f$, $Z = F_s$, $\zeta = \nu$): The maximum of $\overline{S(\nu)}$ in Fig. 3 for a single-symbol OFDM signal defines the correct "sampling" frequency $\nu = 0$ for the chosen subcarrier m. Because ICI-free OFDM reception calls for orthogonal SC spectra (sinc-shaped envelope, $\beta = 0$), the number of neighbors Q must be sufficiently small, and only a few SCs can be included to find a well pronounced maximum in Fig. 3.

3.2 OFDM timing and Nyquist frequency recovery

Complementary to Eq. (1), we now formulate a rect-shaped OFDM baseband signal $s(t)$ in the time domain, or a sinc-shaped Nyquist multi-carrier signal with a rect-shaped spectrum $s(f)$ in the frequency domain [2],

$$\begin{aligned} s_{\mathrm{OFDM}}(t) &= \sum_{i=-\infty}^{+\infty} \sum_{k=0}^{N-1} c_{ik} \exp\left(+\mathrm{j}2\pi \frac{kt}{T_s}\right) \mathrm{rect}\left(\frac{t}{T_s} - i\right), \\ s_{\mathrm{Nyquist}}(f) &= \frac{1}{F_s} \sum_{i=0}^{N-1} \sum_{k=-\infty}^{+\infty} c_{ik} \exp\left(-\mathrm{j}2\pi \frac{kf}{F_s}\right) \mathrm{rect}\left(\frac{f}{F_s} - i\right). \end{aligned} \tag{6}$$

The quantities c_{ik} are again the complex modulation coefficients, T_s is the OFDM symbol duration, and F_s the symbol "duration" in the frequency domain, i.e., the width of the Nyquist bands. The rect-function is defined by:

$$\mathrm{rect}\left(\frac{z}{Z}\right) = \begin{cases} 1 & \text{for} \quad |z| < Z/2 \\ 0 & \text{for} \quad |z| > Z/2 \end{cases} \tag{7}$$

Again, only a finite number of R and Q neighbors with respect to subscripts i and k are considered within the functions Eq. (6) for a given t or f. The signals described by Eq. (6) can

#205525 - $15.00 USD Received 3 Feb 2014; revised 27 Mar 2014; accepted 27 Mar 2014; published 10 Apr 2014

then be formulated in a unified form with $z = t$, $Z = T_s$ (OFDM) or $z = f$, $Z = F_s$ (Nyquist, $\beta = 0$) by

$$s(z) = \sum_{i=-R/2}^{+R/2} c_i(z)\,\mathrm{rect}\left(\frac{z}{Z} - i\right), \quad c_i(z) = \sum_{k=-Q/2}^{+Q/2} c_{ik}\,\exp\left(\mathrm{j}2\pi\frac{kz}{Z}\right). \tag{8}$$

The Fourier series $c_i(z)$ are again represented by a finite number of $Q + 1$ terms subscripted with k due to realization constraints. Figure 4 visualizes the signal Eq. (8) for a single-symbol OFDM signal or for a single-carrier Nyquist spectrum ($R = 0$ and $Q = 2$). In this figure the window width is equal to the symbol width Z in time (OFDM) and frequency (Nyquist).

In the following we show that the ideal time (OFDM) or frequency (Nyquist) receiving window leads to a maximum when averaging the mean signal powers within each window. As before, the goal is to find either the ideal timing for the OFDM time window or the ideal center frequency for the respective Nyquist frequency window. In Fig. 4 this ideal windows would be centered at $z_m = m\,Z,\ m \in \mathbb{Z}$. Again, without loss of generality, we set $m = 0$.

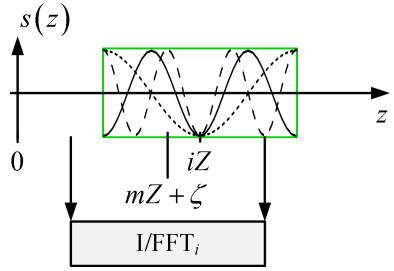

Fig. 4. Signal with a rect-shaped pulse envelope (green) showing either an OFDM signal in time domain or a Nyquist sinc-pulse signal in frequency domain (Eq. (6) for $R = 0$). The black curves show three superimposed "neighbors" (i.e., for $Q = 2$). The coefficients $c_{ik} = c_{0k}$ can be extracted by applying an FFT (for OFDM) or an IFFT (for sinc-pulses). An offset from the ideal I/FFT-window position is defined as ζ.

We now would like to find out to what extent the ideal timing or frequency at $\zeta = 0$ can be found by searching for the maximum in the ensemble average of the signal's mean power $S(\zeta)$ inside the receiving window, i.e., by evaluating

$$\begin{aligned} S(\zeta) &= \frac{1}{Z}\int_{\zeta-Z/2}^{\zeta+Z/2} \left|s(z)\right|^2 \mathrm{d}z, \\ \overline{S(\zeta)} &= \frac{1}{Z}\sum_{i,i'=-R/2}^{+R/2} \overline{\int_{\zeta-Z/2}^{\zeta+Z/2} c_i(z)\,c_{i'}^*(z)\,\mathrm{rect}\left(\frac{z}{Z} - i\right)\mathrm{rect}\left(\frac{z}{Z} - i'\right)\mathrm{d}z} \\ &= \frac{1}{Z}\sum_{i=-R/2}^{+R/2} \overline{\int_{\zeta-Z/2}^{\zeta+Z/2} \left|c_i(z)\right|^2 \mathrm{rect}\left(\frac{z}{Z} - i\right)\mathrm{d}z}. \end{aligned} \tag{9}$$

The rect-shaped symbols for an arbitrary R are non-overlapping, therefore the double sum over $i,\ i'$ reduces to a single sum. If the receiving rect-window with width Z (integration boundaries) coincides with a rect-shaped symbol, we may ignore the rect-function and consequently the sum over i in Eq. (9). This is also true if the receiving rect-window overlaps with two neighboring symbols (no gap between symbols!), as far as the ensemble average is concerned. For an arbitrarily chosen i we then find by substituting $c_i(z)$ from Eq. (8) and by splitting $c_i(z)$ in a z-dependent and a z-independent part,

$$\overline{S(\zeta)} = \sum_{k,k'} \overline{c'_{ik}c'^*_{ik'}}\,\frac{1}{Z}\int_{\zeta-Z/2}^{\zeta+Z/2} \exp\left(\mathrm{j}2\pi\frac{(k-k')z}{Z}\right)\mathrm{d}z = \sum_k \overline{\left|c'_{ik}\right|^2}. \tag{10}$$

#205525 - $15.00 USD Received 3 Feb 2014; revised 27 Mar 2014; accepted 27 Mar 2014; published 10 Apr 2014

Due to inter-symbol interference (ISI), the received coefficients $c'_{ik} \neq c_{ik}$ belong to two different frames and do not correspond to the original data c_{ik}. The orthogonality integral in Eq. (10) reduces the double sum over k, k' to a single sum over k, and because the ensemble average of the modulus-squared coefficients $\overline{|c'_{ik}|^2} = \overline{|c_{ik}|^2}$ is same with and without ISI, Eq. (10) simplifies greatly. As a result, from measuring the average power in a window positioned arbitrarily at $z = \zeta$, we cannot derive any synchronization information.

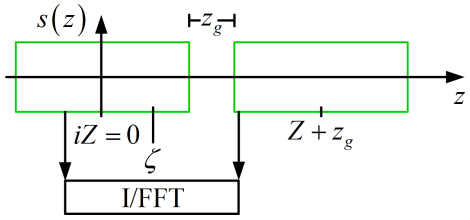

Fig. 5. Rectangular symbols and average power in receiving window as a function of the offset ζ. Signal comprising rect-shaped pulse envelopes (green) either in the time domain (OFDM) or in the frequency domain (Nyquist) separated by a guard interval z_g. The coefficients c'_{ik} are extracted within a rectangular window with an I/FFT.

The situation changes, if next neighbors are excluded, $R = 0$. In this case, the power as given by Eq. (10) drops if the receiving window is positioned wrongly,

$$\overline{S(\zeta)} = \sum_k \overline{|c'_{ik}|^2} \left(1 - \frac{|\zeta|}{Z}\right) \quad \text{for } R = 0 \text{ (no neighbors).} \tag{11}$$

Under this assumption, a peak in the detected triangular-shaped average power $\overline{S(\zeta)}$ of Eq. (11) indicates the optimum window position $\zeta = 0$.

Rather than excluding all neighbors, a small guard interval z_g in time (OFDM) or frequency domain (Nyquist) could be introduced, see Fig. 5. In this case, a peak in the mean power Eq. (11) indicates the optimum position for the chosen window m, even if neighbors are present, $R \neq 0$. To verify this, we compare theory (lines) to simulations (filled squares) in Fig. 6 and find that both agree well. These general results can now be used to perform timing or carrier frequency recovery.

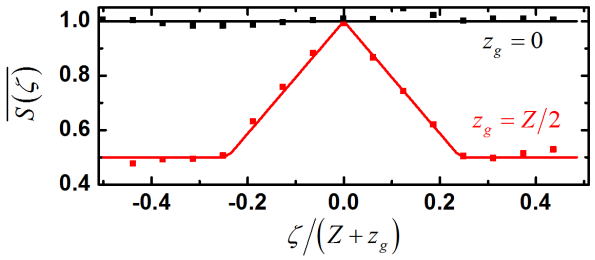

Fig. 6. The ideal OFDM time or the ideal Nyquist frequency window position, respectively, may be found by calculating the ensemble average of the power $S(\zeta)$ within the window as a function of the time/frequency offset ζ. Signals with a guard interval in time or frequency, i.e. with $z_g > 0$, have a distinct maximum exactly at the ideal timing or carrier frequency $\zeta = 0$. Therefore, time window or carrier frequency offsets can only be found for signals with a guard interval. The solid lines show the analytically obtained (Eq. (10) and (11)) results and the solid squares show results obtained by simulations.

Timing recovery for OFDM signals ($z = t$, $Z = T_s$, $\zeta = \tau$, $z_g = t_g$): For a single rectangular OFDM symbol ($R = 0$, not a practical case!), or if a guard interval t_g between adjacent OFDM

#205525 - $15.00 USD Received 3 Feb 2014; revised 27 Mar 2014; accepted 27 Mar 2014; published 10 Apr 2014

symbols exists, the maximum of $\overline{S(\tau)}$ indicates the optimum FFT window position $\tau = 0$. Here, the samples contributing to $\overline{S(\tau)}$ are to be taken from the output of the FFT.

Carrier frequency recovery for Nyquist signals ($z = f$, $Z = F_s$, $\zeta = \nu$, $z_g = f_g$): For a single-carrier Nyquist signal ($R = 0$), or if a spectral guard band f_g exists, the maximum of $\overline{S(\nu)}$ indicates the optimum IFFT window position $\nu = 0$. In this case, the samples contributing to $\overline{S(\nu)}$ are to be taken from the output of the IFFT.

4. Mean modulus algorithm (MMA) and other nonlinear averages for timing and frequency recovery

Evaluation of the MPA $\overline{S(\zeta)}$ for finding the optimum recovery point $\zeta = 0$ does only yield the correct results if certain (sometimes unpractical) conditions are met. More precisely, and with the nomenclature of the previous section, the existence of a distinct maximum requires either sinc-like pulses with raised-cosine spectrum and a certain excess bandwidth $\beta > 0$, or a sufficiently small number of neighbors Q for sinc-shaped pulses/spectra as described by Eq. (5). In analogy, rect-shaped pulses/spectra such as described by Eq. (9) require a temporal or spectral guard interval z_g (or no next neighbor, $R = 0$).

However, in all cases, where evaluation of the mean power fails, one may apply a nonlinear function $f(x)$ [7] to the received samples prior to averaging over a number of L measured values of $S(\zeta)$ in either time (Nyquist) or frequency domain (OFDM),

$$\overline{f(S(\zeta))} = \frac{1}{L}\sum_{l=1}^{L} f(S(\zeta))\Big|_l. \tag{12}$$

In Eq. (12), $f(x)$ can be, e.g., a square root function, a higher order polynomial, an exponential, a logarithm, or even a sinusoidal. Among all these possibilities, using a square root operation (i.e., an absolute-value rectifier) is very convenient as this means averaging over the signals' moduli. This leads us to an algorithm that we will subsequently refer to as the "mean modulus algorithm" (MMA). Computing the modulus and phase of a complex number in Cartesian coordinates is efficiently realized by the so-called CORDIC algorithm [14], where computationally expensive multipliers can be avoided. Furthermore, a transformation to polar coordinates is often employed anyhow when compensating the carrier phase offset, and hence does not consume any additional resources.

In conclusion, the two first moments defined by

$$\overline{S(\zeta)} = \frac{1}{L}\sum_{l=1}^{L} S(\zeta)\Big|_l \qquad (\text{MPA}) \tag{13}$$

$$\overline{\sqrt{S(\zeta)}} = \frac{1}{L}\sum_{l=1}^{L} \sqrt{S(\zeta)}\Big|_l \quad (\text{MMA}) \tag{14}$$

can serve as cost (or objective) functions to efficiently recover timing and frequency information with little computational effort. As shown before, the MPA described by Eq. (13) has a limited area of application. While the MMA, Eq. (14), requires only little additional effort, it can be used to recover timing and frequency information of arbitrary Nyquist and OFDM signals. The wider range of application of the MMA can be attributed to the higher degree of non-linearity when applying a square root operation.

For completeness' sake, we put the MPA and MMA algorithm into the context of other, commonly used algorithms. For instance, the constant modulus algorithm (CMA) [15] is frequently used for polarization demultiplexing. In [2] and [13], it has been shown to also work for recovering frequency and timing information. The CMA cost function is defined by

#205525 - $15.00 USD Received 3 Feb 2014; revised 27 Mar 2014; accepted 27 Mar 2014; published 10 Apr 2014

$$\sigma^2_{\sqrt{S(\zeta)}} = \overline{\left(\sqrt{S(\zeta)} - \overline{\sqrt{S(\zeta)}}\right)^2} = \overline{S(\zeta)} - \overline{\sqrt{S(\zeta)}}^2 \qquad \text{(CMA)}. \tag{15}$$

By rewriting the CMA cost function as per the second term in Eq. (15) it becomes obvious, that the CMA comprises the elements of the MPA and MMA algorithm as introduced in the previous section. The operation of the CMA is well understood for PSK signals, where it can be shown that the variance Eq. (15) is zero at the ideal sampling time $\zeta = 0$. This is valid independent of the pulse shape discussed previously. As an example, for $\zeta = 0$ the sum in Eq. (5) reduces to one term, $\sqrt{S(0)} = |c_0|$, or to $\sqrt{S(0)} = \sqrt{\sum_{k=-Q/2}^{+Q/2} |c_{0k}|^2}$ in the case of Eq. (9). Then, the variance Eq. (15) becomes zero at $\zeta = 0$ and is larger in any other case. For all other QAM formats it is plausible to expect a minimum of the variance at $\zeta = 0$.

Instead of computing the variance of $\sqrt{S(\zeta)}$, one could alternatively evaluate the variance of the signal powers leading to the constant power algorithm (CPA) according to

$$\sigma^2_{S(\zeta)} = \overline{\left(S(\zeta) - \overline{S(\zeta)}\right)^2} = \overline{S^2(\zeta)} - \overline{S(\zeta)}^2 \qquad \text{(CPA)}. \tag{16}$$

If Eq. (16) is used as a cost function instead of the one for the CMA, square root operations can be avoided at the price of additional square operations. However, the general shape of the functions obtained from Eq. (15) and (16) is the same as will be shown later on.

The CMA and CPA cost functions Eq. (15) and (16) are combinations of the MMA and MPA algorithms given by Eq. (13) and (14). And indeed, the functions have been tested and work well for signals with sinc-pulses (Nyquist) or sinc-spectra (OFDM) [2] [13]. However, we are able to show that in most instances it is sufficient and more efficient to work with the MMA of Eq. (14) only. Since the MMA is a subset of the CMA, mathematical operations can be saved, hence reducing computational complexity and latency. In the following, we perform simulations for heavily noise loaded OFDM and Nyquist shaped signals and compare the convergence speed of the CMA and the MMA by determining the number of symbols required for reliable recovery of timing and frequency information. After that, a discussion of limitations and advantages of the exemplarily chosen cost functions Eq. (13)–(16) will be given along with experimental data.

5. Performance of MMA and CMA for noise-loaded signals

To find the number of symbols required to reliably recover timing and carrier information, we simulate QPSK and 16QAM modulated OFDM and Nyquist signals. Noise is added such that the resulting bit error ratio (BER) at the receiver is either 10^{-3} or 10^{-2}. This is close to state-of-the-art hard-decision and soft-decision forward error correction limits. For each BER and each number of received coefficients, timing and frequency information is determined for a 100 times.

#205525 - $15.00 USD Received 3 Feb 2014; revised 27 Mar 2014; accepted 27 Mar 2014; published 10 Apr 2014

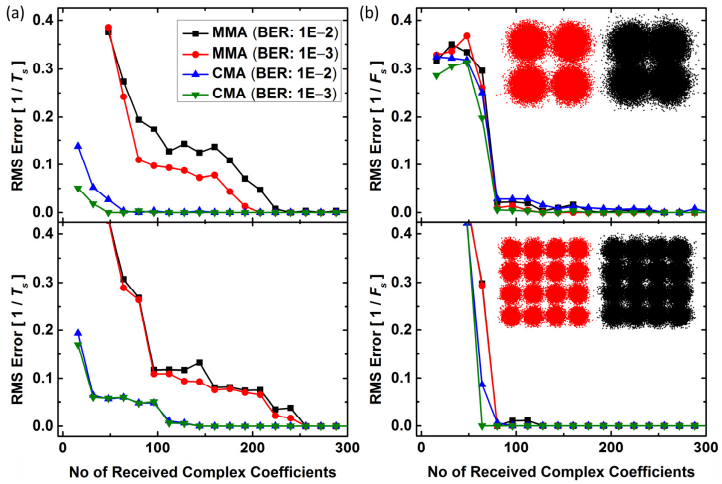

Fig. 7. Performance of MMA and the CMA for simulated QPSK (top) and 16QAM (bottom) OFDM signals with noise loading. (**a**) RMS of error made by (**a**) timing or (**b**) frequency recovery.

We then compute the root-mean-square (RMS) of the error made by the recovery algorithms normalized to either symbol period or bandwidth. Results for OFDM are shown in Fig. 7. In Fig. 7(a) we compare the performance of the MMA and the CMA when being used for timing recovery. It can be seen that the CMA requires less received complex coefficients to reliably determine the FFT window position at the Rx. However, the MMA can handle the increased amount of required coefficients within only two additional clock cycles (assuming a binary adder tree) leading to a net latency and complexity comparable to the CMA where differences between mean modulus and individual moduli have to be summed. When used for OFDM frequency recovery, see Fig. 7(b), both algorithms require the same amount of coefficients.

Results for QPSK and 16QAM Nyquist sinc-pulses are depicted in Fig. 8. Again timing recovery, see Fig. 8(a), and frequency recovery, see Fig. 8(b), is performed with either the CMA or the MMA.

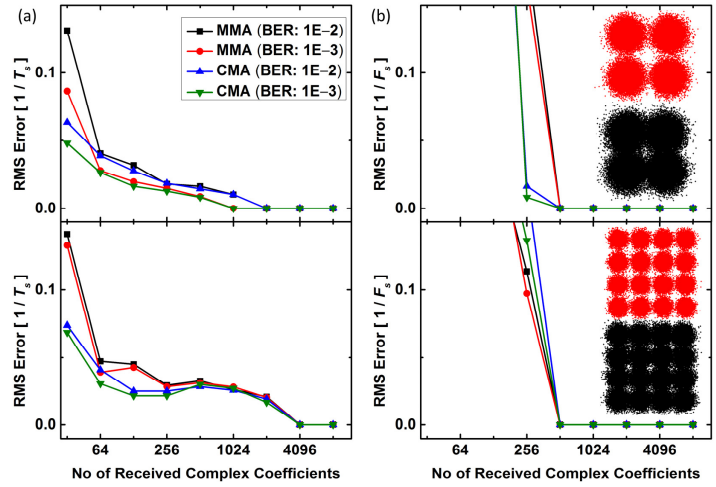

Fig. 8. Performance of the MMA and the CMA for simulated QPSK (top) and 16QAM (bottom) Nyquist signals. (**a**) RMS of error made by (**a**) timing or (**b**) frequency recovery.

#205525 - $15.00 USD Received 3 Feb 2014; revised 27 Mar 2014; accepted 27 Mar 2014; published 10 Apr 2014

From these results we conclude that the proposed MMA and the CMA perform equally well, leaving the MMA with the advantage of less computational complexity except for OFDM timing synchronization where the complexity is virtually same for both algorithms.

6. Experimental setup

The experimental setup is depicted in Fig. 9. A software-defined transmitter (Tx) [16] acts as an arbitrary waveform generator (AWG), i.e., two synchronized field programmable gate arrays (FPGA) store pre-computed waveforms.

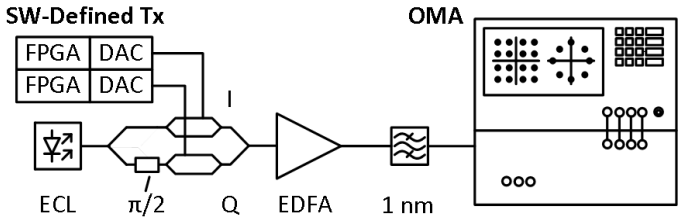

Fig. 9. Experimental setup for transmitting Nyquist or OFDM signals. Two synchronized field programmable gate arrays (FPGA) store pre-computed waveforms and drive attached digital-to-analog converters (DAC). The generated complex waveform is then encoded on an external cavity laser (ECL) with an optical I/Q-modulator. After amplification with an erbium doped fiber amplifier (EDFA) the signal passes a 1 nm-wide bandpass, is coherently received by an optical modulation analyzer (OMA), and processed offline.

With these waveforms the FPGAs drive two Micram digital-to-analog converters (DAC) with a resolution of 6 bit operating at a sampling rate of 28 GSa/s. The in-phase (I) and quadrature (Q) component of the complex Nyquist or OFDM waveforms are encoded on an external cavity laser (ECL) with a center wavelength of 1550 nm. To do so, we use an I/Q-modulator consisting of nested $LiNbO_3$ Mach-Zehnder modulators and a $\pi / 2$ phase shifter. An erbium-doped fiber amplifier (EDFA) amplifies the optical signals. A 1 nm optical band-pass filter removes out-of-band EDFA noise. Finally, an Agilent optical modulation analyzer (OMA) coherently receives the signals using a free-running local oscillator (LO). The in-built real-time oscilloscope samples with a rate of 80 GSa/s. All signal processing is done offline.

7. Experimental results for carrier frequency and timing recovery

To verify the proposed frequency and timing recovery algorithms experimentally, we use the setup depicted in Fig. 9. We transmit Nyquist signals having different roll-off factors β, and ideally rect-shaped OFDM signals. In both cases we employ the formats QPSK, 16QAM (only OFDM) and 64QAM. We evaluate the various cost functions Eq. (13)–(16) and determine either a temporal sampling offset $\zeta = \tau$ or a carrier frequency offset $\zeta = \nu$.

7.1 Orthogonal frequency division multiplexing (OFDM)

We first evaluate the frequency recovery mechanism for OFDM signals comprising 128 SCs, each modulated with QPSK (black), 16QAM (blue), or 64QAM (red).

Carrier frequency recovery ($z = f$, $Z = F_s$, $\zeta = \nu$, $\tau = 0$): We vary the frequency of the LO and extract the modulation coefficients c'_{ik} with an FFT, the window of which is positioned at the ideal synchronization point $\tau = 0$. With the resulting coefficients c'_{ik}, we evaluate the MPA, the MMA, the CMA, and the CPA algorithms according to Eq. (13)–(16) as a function of the frequency offset ν normalized to the subcarrier spacing F_s (symbol rate). The outcome is depicted in Fig. 10. All curves are normalized to their maximum values.

With all methods except for the MPA, the zero offset $\nu = 0$ between the signal's carrier frequency and the LO frequency is found at extremal points, independent of the modulation format, see Fig. 10.

#205525 - $15.00 USD Received 3 Feb 2014; revised 27 Mar 2014; accepted 27 Mar 2014; published 10 Apr 2014

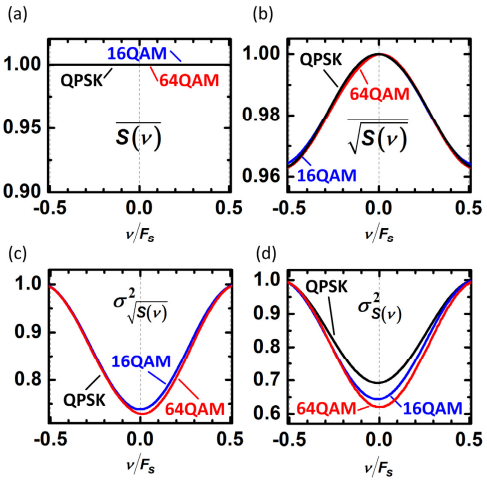

Fig. 10. Experiment showing the performance of four cost functions for OFDM carrier frequency recovery for either QPSK (black), 16QAM (blue), or 64QAM (red) modulated SCs. (**a**) The MPA does not provide an extremum and thus cannot be used to recover the frequency. (**b**) The mean modulus algorithm (MMA) of the extracted coefficients c_{ik} yields a maximum at the frequency offset $\nu = 0$. (**c**) The CMA and (**d**) the CPA provide a minimum for $\nu = 0$.

Timing recovery ($z = t$, $Z = T_s$, $\nu = 0$, $\zeta = \tau$): As a next step we investigate the previously discussed algorithms and the respective cost functions for recovering the timing of OFDM signals. In analogy to the experiment discussed above, we extract the modulation coefficients c'_{ik} for each symbol. This time, however, we fix the frequency offset ν at zero and vary the temporal offset τ of the FFT window. The results are shown in Fig. 11. For Fig. 11(a) only, computing the MPA of simulated OFDM signals with a temporal guard interval τ_g between adjacent symbols gives a distinct maximum where the temporal offset τ equals zero. These results agree well with the predictions made by Eq. (11). In Fig. 11(b)–(d) the temporal window position of measured OFDM signals is evaluated using either the MMA (Fig. 11(b), Eq. (14)), the CMA (Fig. 11(c), Eq. (15)) or the CPA (Fig. 11(d), Eq. (16)). All of these methods can be used as part of a feedback loop that provides a continuous OFDM symbol synchronization.

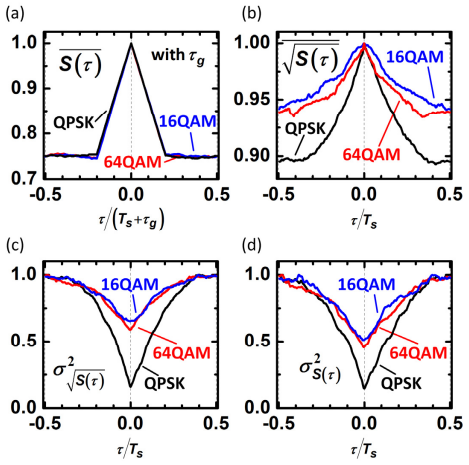

Fig. 11. Demonstration of the performance of four cost functions for OFDM timing recovery. (**a**) MPA cost function for various offset times for simulated OFDM symbols with a temporal guard interval τ_g in-between symbols. (**b**) – (**d**) show the result of applying the cost functions to experimentally obtained OFDM signals using either (b) the MMA, (c) the CMA or (d) the CPA algorithms. These algorithms provide an extremum at the ideal time even if $\tau_g = 0$.

#205525 - $15.00 USD Received 3 Feb 2014; revised 27 Mar 2014; accepted 27 Mar 2014; published 10 Apr 2014

7.2 Nyquist signaling

We now generate QPSK and 64QAM Nyquist signals with different roll-off factors β and investigate the proposed techniques for frequency and timing recovery.

Carrier frequency recovery ($z = f$, $Z = F_s$, $\zeta = \nu$, $\tau = 0$): For frequency recovery, a number of three simultaneous Nyquist signals ($\beta = 0$) centered at different carrier frequencies are transmitted. Only the middle channel is considered while the neighboring Nyquist channels are removed by rectangular digital filters having a pass-band equal to the channel bandwidth. The outcome of the proposed algorithms and cost functions as a function of frequency offset ν is depicted in Fig. 12. For evaluation of the MPA, see Fig. 12(a), we perform simulations and introduce a spectral guard interval ν_g in-between the Nyquist channels. Again, the results agree with the predictions made by Eq. (11), and a distinct maximum can be identified where $\nu = 0$. For the remaining plots the techniques even work without guard intervals. Experiments are again performed with the setup in Fig. 9. It can be seen that the evaluation of the MMA yields a maximum at $\nu = 0$, see Fig. 12(b) and Eq. (14). Furthermore, the CMA, Fig. 12(c), and the CPA, Fig. 12(d), both show a minimum if the LO frequency is synchronized to the carrier frequency of the Nyquist signal.

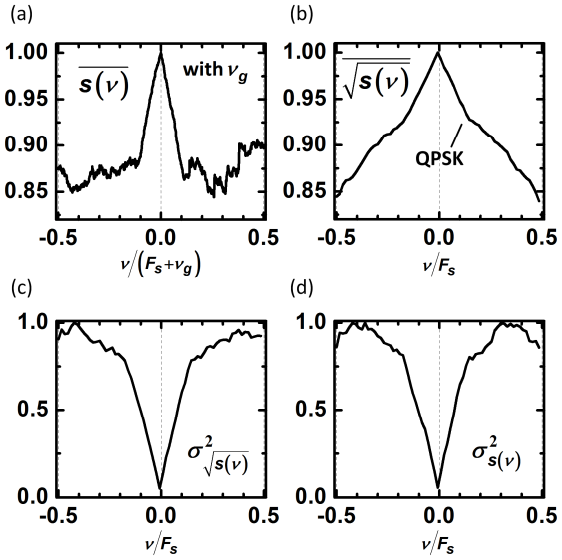

Fig. 12. The performance of four cost functions for Nyquist carrier frequency recovery. (**a**) MPA cost function as a function of frequency offsets applied to a simulated Nyquist signal with spectral guard interval ν_g in-between channels. (**b**) – (**d**) Results of cost functions obtained by applying the operations on experimentally received Nyquist signals without a guard interval using either (b) the MMA, (c) the CMA or (d) the CPA algorithms.

Timing recovery ($z = t$, $Z = T_s$, $\nu = 0$, $\zeta = \tau$): For evaluation of the timing recovery, we transmit single-channel Nyquist signals using "raised-cosine" pulse-shapes Eq. (2) with different roll-off factors β, modulated with either QPSK or 64QAM. The results are shown in Fig. 13. In each of the subfigures Fig. 13(a) and (b) we depict the mean power (MPA, upper left), the mean modulus (MMA, upper right), the variance of the modulus (CMA, lower left), and the variance of the modulus squared (CPA, lower right) as a function of the temporal offset τ from the ideal sampling positions. All cost functions can be used to find the proper sampling times for QPSK, see Fig. 13(a), and 64QAM signals, see Fig. 13(b). However, as predicted by Eq. (5), employing the MPA is not useful for finding the proper timing if signals with $\beta < 0.3$ are received. The curves obtained with Eq. (14) (MMA) show a pronounced maximum at $\tau = 0$ even for $\beta = 0$, and for large supports Q. For Nyquist signals with $\beta > 0.3$, both methods based on the variance (CMA and CPA) fail for high order M-ary QAM. In these scenarios the MPA or the MMA should be used. In Fig. 13(c) we depict measured

#205525 - $15.00 USD Received 3 Feb 2014; revised 27 Mar 2014; accepted 27 Mar 2014; published 10 Apr 2014

constellation diagrams for QPSK and $\beta = 0$ (top) and for 64QAM and $\beta = 1$ (bottom). Sampling with $\tau = 0$ yields the red symbols, whereas sampling with $\tau \neq 0$ will result in the black inter-symbol transitions, i.e., sampling is done at the slope of the sinc-function. The discussed timing recovery for Nyquist signals is robust with respect to carrier frequency and carrier phase offsets since the phase information is not regarded. Furthermore, the methods have shown to tolerate differential group delays >100 ps.

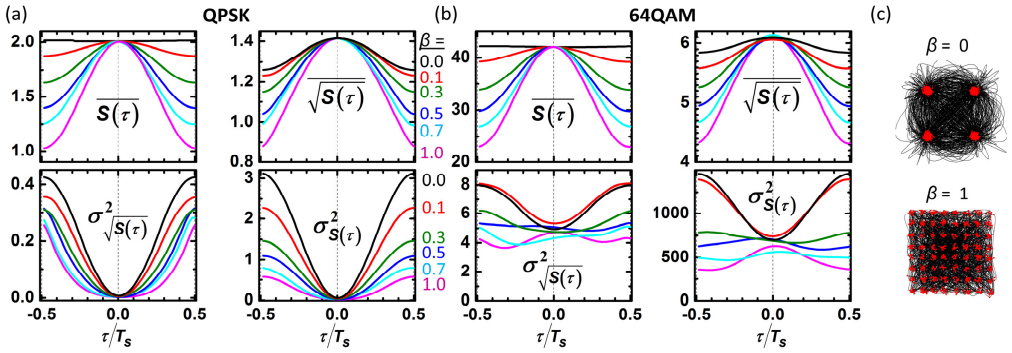

Fig. 13. Performance of four cost functions to recover the timing offset for Nyquist signals with different roll-off factors β. We evaluate the MPA (upper left), the MMA (upper right), the CMA (lower left), and the CPA (lower right) for (**a**) QPSK and (**b**) 64QAM encoded Nyquist signals and as a function of the temporal sampling offset τ. The MPA only yields a good measure for $\beta > 0.1$. Another limitation arises for Nyquist signals with large β where the CMA and CPA algorithms do not provide a distinct minimum for $\tau = 0$ (e.g. for 64QAM). (**c**) Constellation diagrams for QPSK and $\beta = 0$ (top) and for 64QAM and $\beta = 1$ (bottom). Sampling with $\tau = 0$ yields the red symbols whereas sampling with $\tau \neq 0$ results in the black inter-symbol transitions.

8. Carrier phase recovery

After frequency and timing recovery, we still need to compensate for the phase offset φ between the signal carrier and the LO. To do so, the Viterbi-Viterbi algorithm [11] is typically employed. Unfortunately, the computational effort scales with the degree of phase modulation so that especially for high order M-ary QAM with μ different phases a significant amount of computational effort is required (the complex valued signal has to be taken to the power of μ). As a low-complexity alternative we suggest to apply the mean modulus algorithm (MMA) to the real and imaginary parts of the received symbols according to

$$\begin{aligned}
&\overline{\left|\Re\{s(\varphi)\}\right| + \left|\Im\{s(\varphi)\}\right|} = \frac{1}{M}\sum_{m=1}^{M}\left[\left|\Re\{c_m e^{j\varphi}\}\right| + \left|\Im\{c_m e^{j\varphi}\}\right|\right], \\
&c_m = |c_m| e^{j\theta_m}, \\
&\Re\{c_m e^{j\varphi}\} = |c_m|\left[\sin(\theta_m)\sin(\varphi) - \cos(\theta_m)\cos(\varphi)\right], \\
&\Im\{c_m e^{j\varphi}\} = |c_m|\left[\sin(\theta_m)\cos(\varphi) + \cos(\theta_m)\sin(\varphi)\right].
\end{aligned} \tag{17}$$

The outcome predicted by Eq. (17) has been compared to simulations. The results are illustrated in Fig. 14. It can be seen that the MMA provides the ideal phase at the maximum. Figure 14 also shows that Eq. (17) (solid lines) and simulations (squares) coincide. We evaluated QPSK, Fig. 14(a), 16QAM, Fig. 14(b), 32QAM, Fig. 14(c), and 64QAM data, see Fig. 14(d). Insets show constellation diagrams with different phase offsets φ. While the Viterbi-Viterbi algorithm requires a significant amount of multipliers, the algorithm according to Eq. (17) does not require any multipliers at all and is thus highly beneficial for implementations with emphasis on low computational effort. As with the Viterbi-Viterbi algorithm, there is a phase ambiguity as the received constellation could be rotated by

#205525 - $15.00 USD Received 3 Feb 2014; revised 27 Mar 2014; accepted 27 Mar 2014; published 10 Apr 2014

multiples of π / 2 (for quadratic constellations) [11]. This has to be handled separately, e.g., by training symbols.

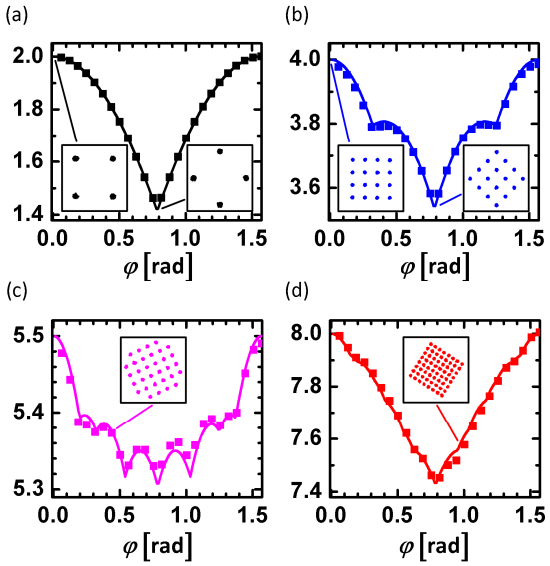

Fig. 14. Carrier phase estimation by applying the MMA to the real and imaginary values of the signal: Theory (lines, Eq. (17)) and simulations (squares) agree well. Typically, an offset φ between signal carrier phase and LO phase is observed. Constellation diagrams for different φ are shown as insets. (**a**) QPSK. (**b**) 16QAM. (**c**) 32QAM. (**d**) 64QAM.

9. Conclusions

Efficient algorithms to recover carrier and timing information of optical Nyquist and OFDM signals were proposed and theoretically discussed. These techniques include the evaluation of the mean power (MPA), the mean modulus (MMA), the variance of the moduli (CMA), the variance of the moduli squared (CPA), and the MMA of real and imaginary parts. It has been shown, that the MMA is a highly efficient method to derive frequency and timing information in all instances of practical relevance. In addition, we show that the MMA can be used to recover the phase simply by adding the moduli of real and imaginary parts. The MMA is efficient, provides low latency and thus enables an implementation in a feedback loop for a continuous control at highest speed. We verified our findings with both simulations and experiments comprising high-speed optical OFDM and Nyquist signals.

Acknowledgments

This work was supported by the projects FOX-C, Piano + OTONES, by Micram Microelectronic GmbH, OFS, as well as by the Xilinx University Program (XUP), and by the Agilent University Relations Program. We further acknowledge financial support by Karlsruhe School of Optics & Photonics (KSOP), and by Deutsche Forschungsgemeinschaft and Open Access Publishing Fund of Karlsruhe Institute of Technology (KIT).

#205525 - $15.00 USD Received 3 Feb 2014; revised 27 Mar 2014; accepted 27 Mar 2014; published 10 Apr 2014